NUMERICAL SIMULATION OF THE EXPERIMENT ON TURBULENT MIXING AFTER MULTIPLE SHOCK WAVE PASSAGES ACROSS INTERFACE

Sin'kova O.G., Statsenko V.P., Yanilkin Yu.V., A.R. Guzhova, Pavlunin A.S.

Paper to be presented at the International Workshop on Physics of Compressible Turbulent Mixing (Cambridge, July 2004)

The paper gives results of direct numerical simulation of turbulence at the interface of two various gases in shock tube caused by interaction with shock waves. Computations were carried out using hydrodynamic 3D TREK code /1/.

Computation results were processed (averaged) to determine the mixing zone width evolution and mean-square fluctuations of velocity components within it.

The calculated results are compared to the corresponding data of experiments /2-3/ carried out by French scientists, who obtained principally new results. They were the first who performed regular measurements of instant flow velocity values in turbulent mixing zone (TMZ). It has been found how fluctuations of the longitudinal component of mass flow velocity evolve in TMZ before and after interaction with shock waves reflected from the shock tube's end. Statistical averaging over the results of multiple measurements gave time dependences for mean-square fluctuations of the longitudinal velocity components at five Eulerian points. In earlier experiments, only the TMZ width dependence on time and mean density distribution were measured.

The essence of the experiment consists in the following: a vertical shock tube with cross-section 8cm and of length 120 cm was filled out with two gases (SF_6 from below and air from above), initially separated by a plastic membrane of thickness 0.3 nm. The initial distance between the gas-gas interface (membrane) and rigid wall was 30 cm. Constant pressure 2.15 bar was implemented at the other end of the shock tube and moved through SF_6. With the shock wave arrival at the interface Riemann problem rises that results in a rarefaction wave propagating through SF_6, while the shock wave continues moving in air. The shock wave is then reflected from the rigid wall and moves towards TMZ, and afterwards it moves towards the rigid wall again. Thus, the TMZ growth is the result of its interaction with a series of shock waves reflected from the tube's end.

In the experiment, a lattice made of thin wire was placed near the membrane to generate initial perturbations; after a shock wave had passed the membrane moved towards the lattice and failed on it resulting in an initial zone of turbulence development.

1 Setting up computations

Fig.1 shows the geometry of 3D computations. Unlike the experiment, the tube cross-section is 5cmx5cm.

Air and SF_6 are considered to be ideal gases with adiabatic exponents 1.4 and 1.094, respectively. The initial densities are 0.0012 g/cm^3 for air and 0.006 g/cm^3 for SF_6. Boundary conditions are "rigid walls" for all edges.

A series of three computations was carried out (see Table 1). In each of the computations above, the computational grid was uniform along axes OX and OY and along 0<z<30cm; within the range 30 < z< 120 the grid had geometric ratio q=1.0063 (400 cells in computations 1 and 2, and 600 cells in computation 3).

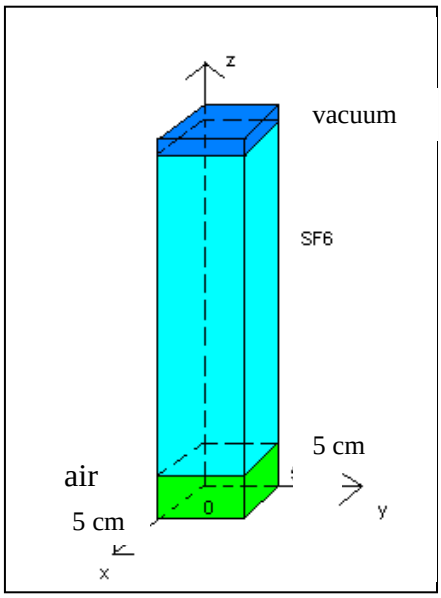

Fig.1. The initial geometry

Table 1 – Variations of computations

Variant No.	Number of cells $N_x x N_y x N_z$	$h_x x h_y$	h_z 0<z<30
1	100x100x1002	0.05x0.05	0.05x0.05
2	100x100x1002	0.05x0.05	0.05x0.05
3	150x150x1502	0.03x0.03	0.03x0.03

In each of the computations above, the computational grid was uniform along axes OX and OY and along 0<z<30cm; within the range 30 < z< 120 the grid had geometric ratio q=1.0063 (400 cells in computations 1 and 2, and 600 cells in computation 3).

Various ways of generating initial perturbations of density at the interface (z = 30см) were used. If perturbations are not specially specified, they occur because of the computational scheme's non-monotone behavior and reach high values before the shock wave arrivals at the interface. In this case, turbulent mixing appears to be knowingly overestimated after the shock wave has passed across the interface. In computation 1 the velocity was zeroed (near the interface, on the side of the heavy gas) every 0.01 ms till t=3.5 ms and within the range from t=3.5 ms to t=4.4 ms it was zeroed every time step. At time t=4.4 ms (the time of the shock wave arrival at the interface) zeroing was stopped.

Thus, no perturbations were intentionally specified in computation 1. In computation 2 zeroing of velocity perturbations at the interface is performed every time step, however, at time t=4.4 ms, before the shock wave arrivals at the interface (the interface remains unperturbed and for this reason perturbations are intentionally specified) random perturbations of density are generated near it in the layer 4 cells thick: $\delta\rho = \rho \pm (\rho_2 - \rho_1)/5$, density ρ in these four cells was linearly pre-interpolated.

In computation 3 the algorithm of specifying perturbations at the interface is the same as in computation 2, however, a finer computational grid is used.

2 3D computation results

Fig. 2 shows the position of TMZ boundaries versus time. The 3D computation results, as one can see, are quite close to each other thereby proving that there is no significant effect of the chosen way of specifying perturbations and the number of computational cells in use on the TMZ width. There is a good agreement with the experimental data.

Fig.2 also shows R-t diagram of shock waves. It is clearly seen that three shock waves reflected from the rigid wall pass through TMZ. Note that significant growth of the TMZ width takes place during propagation of the first shock wave reflected from the rigid wall ($t_{r1}\approx 5.8$), however, the TMZ growth becomes even more intensive during propagation of the second reflected shock wave ($t_{r2}\approx 6.4$).

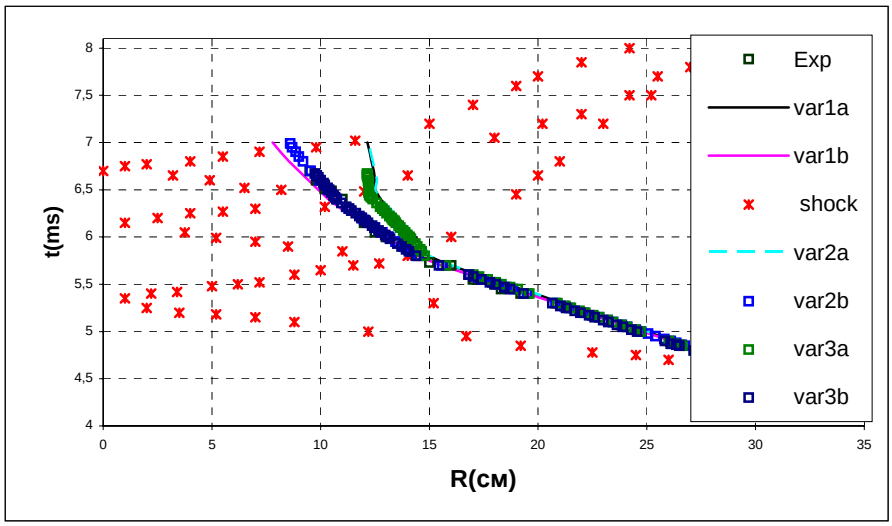

Fig. 2. R-t diagram of shock waves and TMZ boundaries

In the experiments described in [2-3] fluctuations of the longitudinal velocity components were measured using five detectors. The correspondence between the coordinates of detectors in the experiments and notations adopted for computations is as follows: d_498 – 24.9 cm, d_349 – 17.45 cm, d_278 – 13.9 cm, d_262 – 13.1cm, d_242 – 12.15 cm.

In Figs.3-7 below, time dependences of the squared fluctuations of longitudinal velocity component, $< u_z'^2 >$ calculated for the detectors above are shown. Averaging is performed in plane XY corresponding to the shock-tube's cross-section.

The difference in the calculated values of $< u_z'^2 >$ between all the variants of computations is insignificant, while the maximums for detectors 498 and 349 are by an order and a half lower than those measured during the experiment. This is clear with regard to fact that at the times of maximums for these detectors (d498- t_1= 4.95, d349- t_2=5.5) the calculated TMZ widths (in computation 2) are L_1=0.25cm and L_2=0.5cm, i.e. 5 and 10 computational cells, respectively. These

values are insufficient, of course, to give valid description of turbulence during this phase, because of the mean directed flow velocity behind the wave front.

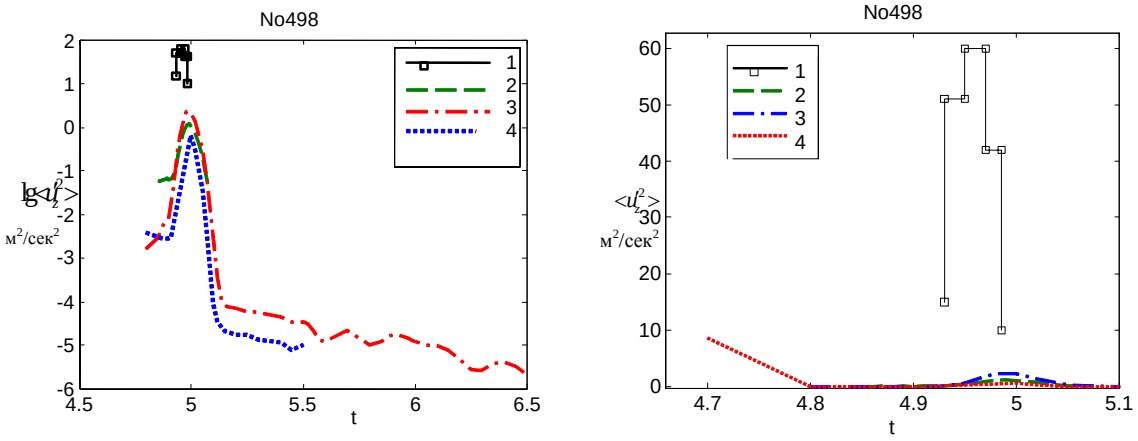

Fig. 3. Squared fluctuation of longitudinal velocity component versus time for d_498: 1 - experiment, 2-4 – computations 1-3, respectively

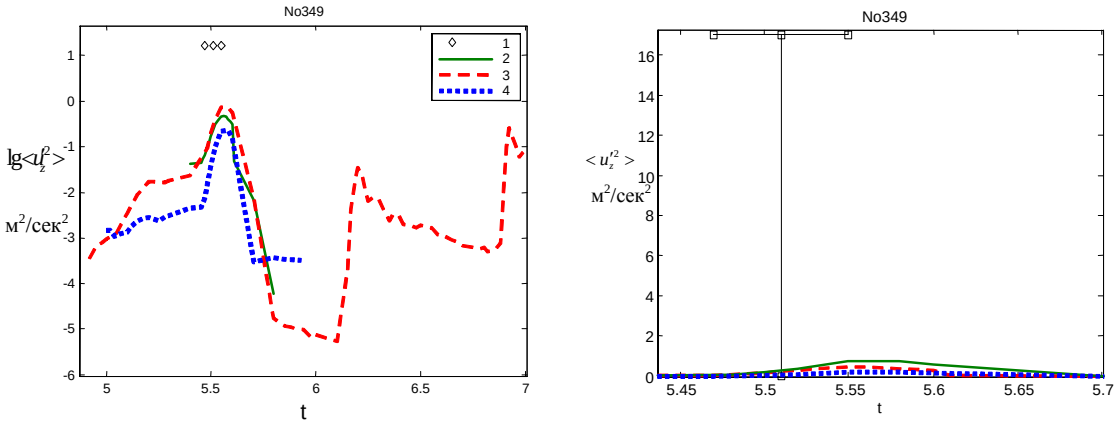

Fig. 4. Squared fluctuation of longitudinal velocity component versus time for d_349: 1 - experiment, 2-4 – computations 1-3, respectively

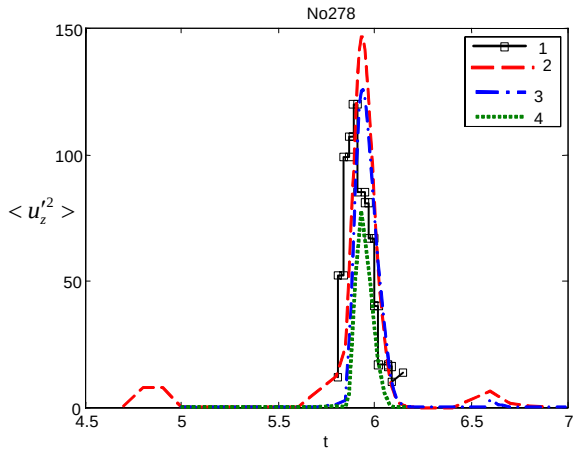

Fig. 5. Squared fluctuation of the longitudinal velocity component versus time for d_278: 1 - experiment, 2-4 – computations 1-3, respectively

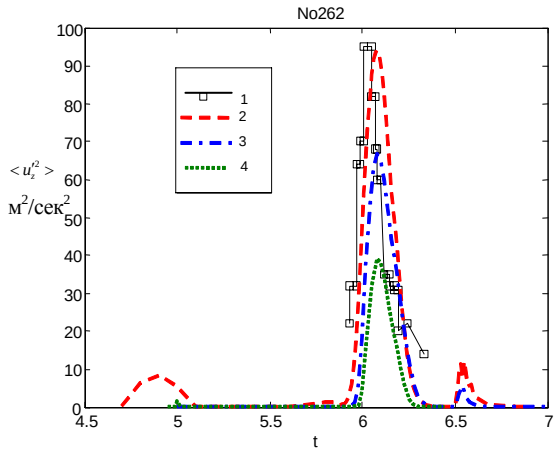

Fig. 6. Squared fluctuation of the longitudinal velocity component versus time for d_262: 1 - experiment, 2-4 – computations 1-3, respectively

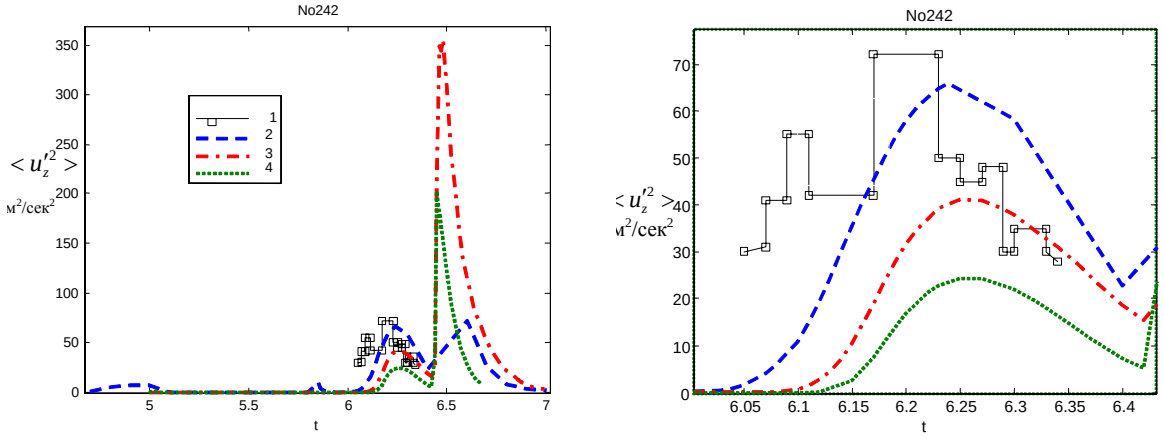

Fig. 7. Squared fluctuation of the longitudinal velocity component versus time for d_242:
1 - experiment, 2-4 – computations 1-3, respectively

Indeed, TREK code uses the difference scheme of the first order of approximation. The value of scheme viscosity of this code in case of quasi-stationary flows (the type of flow behind the wave front) can be estimated using the following equations for momentum transfer:

$$\frac{\partial \rho u_x}{\partial t} + div \rho u_x \vec{u} + \frac{\partial P}{\partial x} = \frac{\partial}{\partial x}\left(\frac{h}{4}\rho u_x \frac{\partial u_x}{\partial x}\right) + \frac{\partial}{\partial y}\left(\frac{h}{4}\rho u_y \frac{\partial u_x}{\partial y}\right) + \frac{\partial}{\partial z}\left(\frac{h}{4}\rho u_z \frac{\partial u_x}{\partial z}\right) + \theta_1\left(h^2, \tau^2\right),$$
$$\frac{\partial \rho u_y}{\partial t} + div \rho u_y \vec{u} + \frac{\partial P}{\partial y} = \frac{\partial}{\partial x}\left(\frac{h}{4}\rho u_x \frac{\partial u_y}{\partial x}\right) + \frac{\partial}{\partial y}\left(\frac{h}{4}\rho u_y \frac{\partial u_y}{\partial y}\right) + \frac{\partial}{\partial z}\left(\frac{h}{4}\rho u_z \frac{\partial u_y}{\partial z}\right) + \theta_2\left(h^2, \tau^2\right), \quad (1)$$
$$\frac{\partial \rho u_z}{\partial t} + div \rho u_z \vec{u} + \frac{\partial P}{\partial z} = \frac{\partial}{\partial x}\left(\frac{h}{4}\rho u_x \frac{\partial u_z}{\partial x}\right) + \frac{\partial}{\partial y}\left(\frac{h}{4}\rho u_y \frac{\partial u_z}{\partial y}\right) + \frac{\partial}{\partial z}\left(\frac{h}{4}\rho u_z \frac{\partial u_z}{\partial z}\right) + \theta_2\left(h^2, \tau^2\right).$$

The right-hand sides of equations (1) can be treated as derivatives of stress “tensor” components of approximation viscosity, they can be written as

$$\sigma_{ik} = \frac{1}{4} h \rho u_k \frac{\partial u_i}{\partial x_k}, \quad (2)$$

where u_k is the typical flow velocity. We use “tensor” in invert commas, because neither equation (1), nor equation (2) are tensors.

Nevertheless, formula (1) is similar to the expression for viscous stress tensor components in Navier-Stokes equations. Here, the scheme viscosity coefficient being a vector depending on the flow velocity and the computational cells size, h,

$$\mu_{ck} = \frac{1}{4} h \rho u_k, \quad \nu_{ck} = \frac{1}{4} h u_k \quad (3)$$

plays the role of molecular viscosity coefficient.

With the shock wave arrival at the interface, the mass velocity has actually one component, u_z, the other two components, u_x and u_y , can be neglected.

Thus, the scheme viscosity coefficient can be written as

$$\nu_{cz} \approx \frac{1}{4} h < u_z > . \qquad (4)$$

Substitution for real values $<u_z>=u_r \approx 12.5$cm/ms and h=0.05cm in formula (4) gives $\nu_{cz} \approx 0.15\,\text{cm}^2/\text{ms}$.

Use formula $L = \sqrt{\nu_{cz}(t - t_0)}$ to calculate the expected TMZ width, where t_0=4.55 ms is the time of shock wave arrival at the interface, t_1 = 4.95ms is the time of maximum for detector 498 in computation 2, t_2= 5.50 ms is the time of maximum for detector 349 in computation 2.

We now have the estimate for purely schematic smearing of the turbulent zone along z coordinate: $L_1 \approx 0.23$cm (L_1=0.25cm in computation for detector 498 (24.9cm)), $L_2 \approx 0.56$cm (L_2=0.50cm in computation for detector 349 (17.45cm)), the result is close to the data given above for this computation.

The maximum values of mean-square fluctuations of the longitudinal velocity component are $u_{t1} \approx 0.8\,\text{cm/ms}$ for d498 (24.9cm) and $u_{t2} \approx 0.4\,\text{cm/ms}$ for d349 (17.45cm), this means that the longitudinal component of turbulent energy attenuates.

Note that situation with the shock wave propagating from the rigid wall out of the heavy substance into the light one is more stable. A typical scale of turbulence in space, l_t should be noticeably smaller than the width of TMZ, L. Assuming that $l_t = L$ is the maximum estimate we obtain the turbulent viscosity coefficient $D_t \sim l_t u_t$. In order to estimate the value of this quantity for the first two detectors, d498 and d349, put the corresponding values for d498 - l_t = 0.23 cm and u_t = 0.80 cm/ ms - into this formula and obtain D_t = 0.18 cm^2/ms and, similarly, for d349: l_t = 0.56 cm and u_t = 0.40 cm/ms give D_t = 0.22 cm^2/ms. These values are comparable with ν_c = 0.15 cm^2/ms.

Thus, the scheme viscosity will strongly suppress the longitudinal component of turbulence energy.

Besides, stability is observed in the moving system after the first shock wave has passed through and turbulent mixing in this phase will be suppressed according to this process physics.

The situation is absolutely different at time 5.4ms<t<6.4ms after the first reflected (from the rigid wall) shock wave has passed through TMZ. The mass velocity behind the shock front decreases in this case: $< u > \approx 4$cm/ms. Accordingly, the scheme viscosity decreases: $\nu_c \approx 0.05\text{cm}^2/\text{ms}$. At the same time, physically unstable conditions are observed at the interface because of the shock wave passed from the light substance into the heavy one.

Indeed, as one can see in Fig.5, detector d-278, the closest to TMZ position (at time t=5.4ms), recorded the maximum value $< u_z'^2 > = 120\text{m}^2/\text{s}^2$ at a later time t=5.9 ms.

Detector d-262, the more distant one from the above-mentioned TMZ position, recorded the maximum value $< u_z'^2 >$ =95m^2/s^2 at an even later time t=6 ms (see Fig.6).

And, finally, detector d-242, the most distant form the TMZ position above, recorded the maximum $< u_z'^2 >$ =72m^2/s^2 at time t=6.2 ms, i.e. later than the other detectors, as it is clearly seen in Fig.7. Thus, for time $\Delta t \approx 0.3$ms (from time t=5.9ms to t=6.2ms) the maximum value of $< u_z'^2 >$ decreased by a factor of 1.67 in this case, while for detectors d-349 and d-498 the corresponding maximum value of $< u_z'^2 >$ decreased by a factor of 3.53 for time $\Delta t \approx 0.5$ms (from time t=4.9ms to t=5.4ms), i.e. attenuation of turbulence was less intensive.

Besides a scheme viscosity decrease, there is an increase of TMZ width that is an increase of the number of computational cells in TMZ. This allows us to give correct description of turbulence.

Note, however, that we have the results of measurements made during the experiment till time $t \le 6.34$ ms, while in computations for detector d-242 we observe the second maximum at time t=6.5 ms which is higher than the first one and equals $< u_z'^2 >$ =356 m^2/s^2. This is because at that time the detector is inside TMZ through which the second shock wave reflected from the rigid wall has passed.

A similar maximum, however, a smaller one (as it should be expected) and at a later time $t \approx 6.55$ ms is observed for detector d-262 located near the very brink of TMZ at that time.

An even smaller maximum and at an even later time $t \approx 6.6$ ms is observed in computations for detector d-278 located behind TMZ at the time of interest.

3 Results of computations using Nikiforov model

Fig. 8 shows R-t diagram of shock waves and the curve of TMZ position versus time obtained in computations using Nikiforov model implemented in EGAK code complex. (Earlier, similar computational investigations using this model were carried out by VIKHR' (Vortex) code [5]). The agreement between the latter and the computations described in [2-3] is good enough, in general, though it is worse than for 3D computations (Fig.2).

Figs.9-11 show comparison between time dependences of mean-square fluctuations of the longitudinal component of mass velocity obtained using Nikiforov model and the results of direct 3D numerical simulation given above. In general, the agreement between computations with Nikiforov model and the data of experiments [2-3] is satisfactory, however, it is worse than for the results of 3D computations.

In computations using Nikiforov model for detector d-278 through which TMZ passes at the time of its interaction with the first, most intensive shock wave reflected from the shock tube end the maximum value of velocity fluctuations exceeds, by a factor of 2, the experimentally measured

value. This means the Nikiforov model gives slightly incorrect description of the behavior of turbulence in the area of large gradients of mean gas dynamic values.

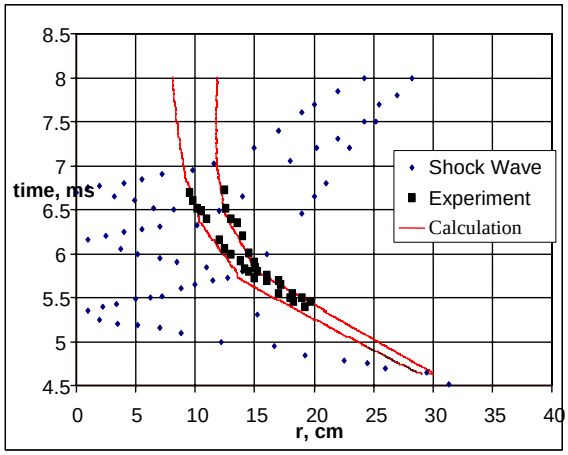

Fig..8. R-t diagram of shock wave and TMZ boundaries

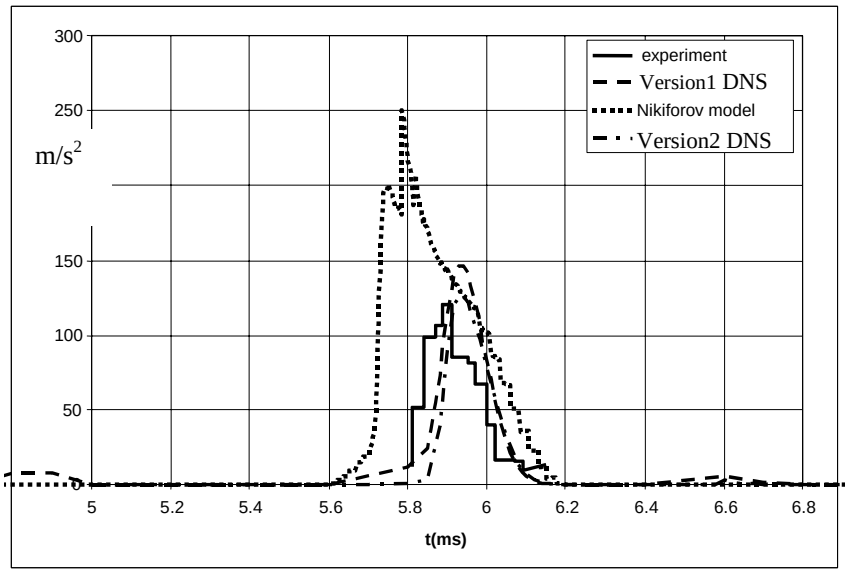

Fig. 9. Squared fluctuations of the longitudinal velocity component versus time for detector 278 (13.9 cm) in computations using Nikiforov model and in versions 1, 2 of computations with direct numerical simulation method

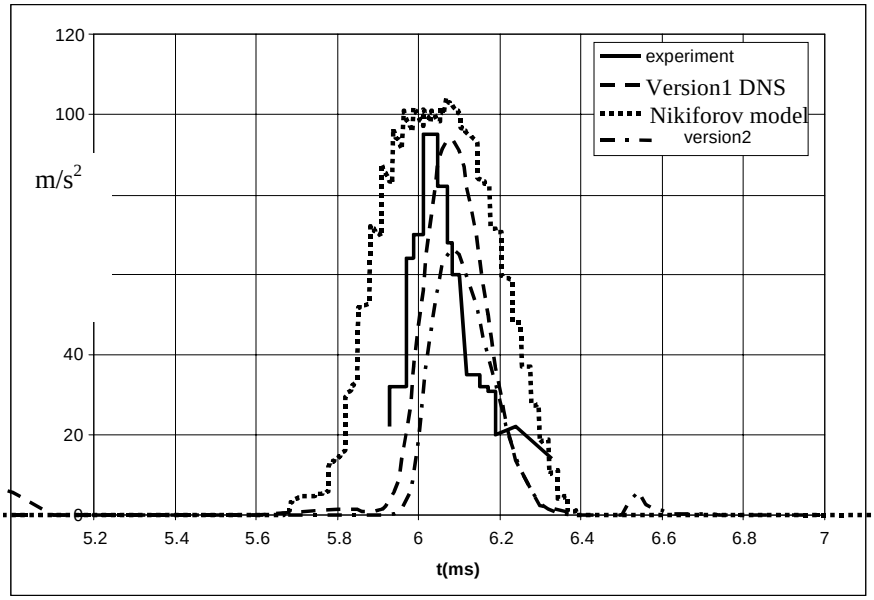

Fig.10. Squared fluctuations of the longitudinal velocity component versus time for detector 262 (13.1 cm) in computations using Nikiforov model and in versions 1, 2 of computations with the direct numerical simulation method

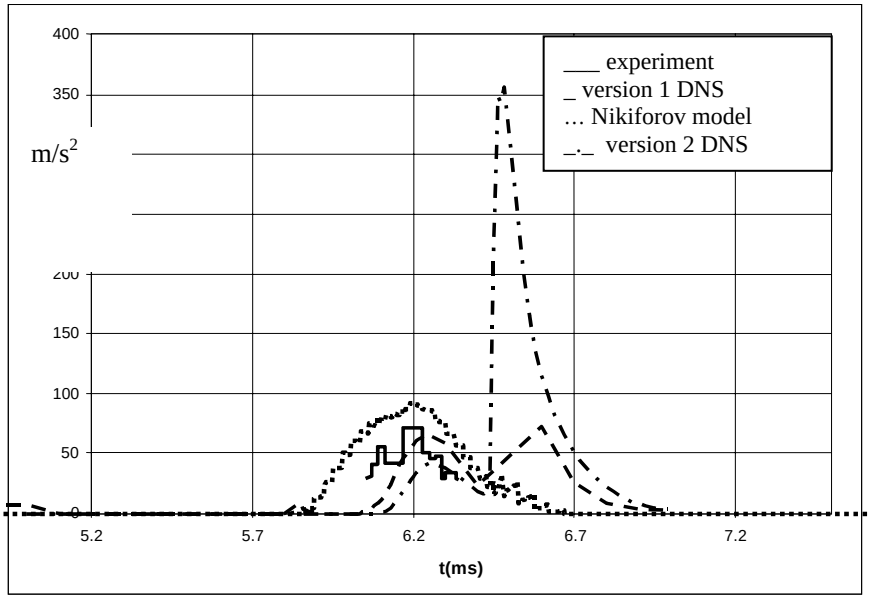

Fig. 11. Squared fluctuations of the longitudinal velocity component versus time for detector 242 (12.15 cm) in computations using Nikiforov model and in versions 1, 2 of computations with the direct numerical simulation method

Conclusion

3D computation results are close, in general, to the data of experiments. The method of specifying perturbations and the number of computational cells insignificantly affect, in practice, the TMZ width. It is worth to note that almost full coincidence of TMZ boundaries located in SF_6 is observed for all computations. Significant growth of the TMZ width takes place during propagation of the first shock wave reflected from a rigid wall. However, TMZ is growing more intensively during propagation of the second reflected shock wave.

When the mixing zone associated with air/SF_6 interface moves across detectors d-242, d-262, and d-278, it has a noticeable width. For these detectors, the calculated time dependence of the squared longitudinal velocity component fluctuations, $< u_z'^2 >$ agrees, in general, with the results of measurements [2,3].

The other two detectors, d-349 and d-498, are at a longer distance to the wall, the mixing zone passing across them is of an insignificant width. For these detectors, the calculated value of $< u_z'^2 >$ is significantly lower than the experimentally measured value. The paper shows that such difference can be attributed to the scheme viscosity effect.

In general, the agreement between the results of computations using Nikiforov model and the experimental data [2-3] seems to be satisfactory, though it is worse than for 3D computation results.

References

1. A.L.Stadnik, A.A.Shanin, Yu.V.Yanilkin. Eulerian code TREK for computation of 3D hydrodynamic multicomponent fluids // VANT. Ser.: Math.Model.Phys.Proces., 1994, Issue 4.
2. F. Poggi, M-H. Thorembey, G.Rodriguez. Velocity measurements in gaseous mixtures induced by Richymyer-Meshkov instability // Physics of Fluids. 1998. Vol.10, No.11. pp. 2698-2700.
3. D. Souffland, O Gregoire, S. Gauthier, F. Poggi, J.M. Koenig. Measurements and simulation of the turbulent energy levels in mixing zones generated in shock tubes// 6th International Workshop on the Physics of Compressible Turbulent Mixing, Marseille, France, 1997. pp. 486-491.
4. V.A.Andronov, S.M.Bakhrakh, E.E.Meshkov, V.V.Nikiforov, A.V.Pevnitskii, A.I.Tolshmyakov. Experimental investigation and numerical simulation of turbulent mixing in 1D flows. DAN SSSR, 1982, V.264, No.1, pp.76-82.
5. V.I.Kozlov, A.N.Razin. The behavior of mean squared velocity fluctuations during TMZ interaction with shock waves. //VANT. Ser.: Math.Model.Phys.Proces.2001. Issue. 3. pp.3-8.